UDC 519.23:621.391.8

I. DJUROVIC [1,2], V. LUKIN [3], A. ROENKO [3]

[1] *University of Montenegro, Electrical Engineering Department, Montenegro*
[2] *Institute for Cutting Edge Information and Communication Technologies, Montenegro*
[3] *National aerospace university named after N. E. Zhukovsky «KhAI», Ukraine*

TIME-FREQUENCY REPRESENTATION ENHANCEMENT: APPROACH BASED ON IMAGE FILTERING METHODS

The task of filtering of the time-frequency representations, obtained by the S-method, using advanced digital image processing filters, both local and nonlocal is considered. Such enhancement is important for design of the time-varying filters for processing of nonstationary frequency modulated signals. The class of local filters is represented by spatial domain filtering using median and related filters. Orthogonal transform based denoising is represented by DCT domain filtering. The block matching 3-D filter is considered as a representative of nonlocal filter class. It is demonstrated that the noise in the time-frequency representations based on S-method has rather complicated nature: non-Gaussian pdf, spatially correlated properties with varying parameters. It is shown that direct application of the considered filters to such a challenging noisy environment is not possible. Then, several filter modifications are proposed and analyzed with respect to integral and local parameters – MSE and MAE. The block matching 3-D filter is shown to provide the best results but at the expense of quality loss in representation of weak components.

Keywords: *Time-frequency representation; S-method; Digital image processing; DCT-based filter; Block matching 3-D filter.*

Introduction

The time-frequency representations (TFRs) can be considered as a mapping of an analyzed signal to 2-D matrix/image indexed with time and frequency coordinates [1, 2]. In this way, it becomes possible to analyze, separate, filter, compress, and process signals/data that are indistinguishable in both time and spectral domains.

There are numerous types of the TFRs that can be roughly divided into the following categories according to the linearity of transform: linear, quadratic, and higher-order representations [3]. Also, transforms can be non-adaptive (with preselected parameters) or adaptive when transform parameters are adjusted somehow to an analyzed signal [4]. A particularly interesting issue is minimization of the noise influence to the TFRs [5]. Existing techniques are mainly focused on noise filtering based on analysis in the spectral domain with thresholding, reassigning, estimating signal parameters, and other techniques applicable in time and frequency [6, 7], or joint time-frequency (TF) domain [8, 9]. Generally, filtering of time-varying signals can be considered as one of the most important applications of the TFR processing.

It has been shown [6] that the standard filtering in time or frequency domain has a limited accuracy for nonstationary frequency modulated (FM) signals. One of the novel approaches which allows further increasing the TFR noise suppression performance while remaining important features of TFR is based on idea to consider TFR as a specific image. Then, it is possible to apply different filtering techniques developed in image processing field [10, 11] for noise removal from TFR. Using this approach, several filters have been proposed for 2-D filtering in the TF domain [12-14]. In the time-varying filtering the most important issue is recognition of the signal components in the TF plane. Then efficient filtering-denoising or signal reconstruction can be performed using procedure from [14].

The first group of filters [12] performs detection of regions of the signal components and masking noise components in the TFR plane. The second group of techniques [13, 14] is based on the switching scheme - commonly two TFRs are considered with different characteristics in rejecting noise and preserving quality of signal components. Then, according to some switching rule, "pixels" of the resulting TFR are selected from two initial TFRs.

Described filter groups have limited accuracy since filtering of a TFR as a 2-D image is rather challenging. Namely, noise in TF images is often signal-dependent and it differs for various TFRs [15]. For example, for the Wigner distribution (WD), noise is Gaussian and signal-independent over entire TF plane [16]. Resulting noise probability density function (pdf) for many other TFRs is closer to the Rayleigh distribution while having signal-dependent behavior [17]. Another common feature of TFR noise is that its variance can be significantly

higher for signal terms than in the regions outside them.

The goal of this paper is to study application of several advanced nonlinear filtering approaches to the task of TFR denoising. First, nonlinear scanning window filters are applied. Filters belonging to the second group of techniques are based on the discrete cosine transform (DCT) since it gives significantly better results comparing to other transforms [18]. Nonlocal filters have become extremely popular in image processing [19, 20]. Therefore the block matching 3-D (BM3D) filter is used as a representative of the third group of techniques [20]. It is shown that these advanced strategies for image filtering can also be used for reducing noise effects in the TFRs with small negative impact to the signal auto-terms.

The paper is organized as follows. Introduction to the well-known TFRs, their interconnection with S-method (SM) and the overview of the noise influence on different TFRs are considered in Section 2.1. Detailed analysis of noise characteristics in the SM is carried out in Section 2.2. Section 3 represents an overview of filtering techniques which can provide the SM denoising effect. The criterions used for estimation the TFR filtering efficiency are described in Section 4. Simulations and detailed analysis of obtained results for each class of filtering techniques are given in Section 5.

1. TFR analysis

1.1. Noise influence on common TFRs

The most popular division of TFRs is based on their linearity [3, 4]. When linear combination of input signals produces linear combination of TFRs, we have linear transform. Among them we can mention the short-time Fourier transform (STFT), Gabor transform, wavelet transform, S-method, etc. [8, 9, 21].

Consider noise influence on the STFT. For discrete-time signal $s(t_n)$, it is defined as:

$$\mathrm{STFT}_s\left(t_n, f_p\right) = \sum_k s\left(t_n + t_k\right) w\left(t_k\right) \exp\left(-j2\pi f_p t_k\right), \quad (1)$$

where $w(t_k)$ is a window function that is commonly symmetric $w(t_k)=w(-t_k)$ and decreasing from the origin $w(|t_k|) \le w(|t_l|)$ for $|t_k| > |t_l|$,

t_n and f_p denote a discrete time and frequency samples equaled to $t_n=t_{st}+nT_S$ and $f_p=pF_S/N$,

t_{st} is the start time,

$p \in [1;N]$, $N=512$,

T_S denotes a sampling interval, $T_S=T/N=1/F_S$,

T is a duration of observation interval.

For signal corrupted by the additive white Gaussian noise (AWGN), $\xi(t_n)$, with zero mean and standard deviation (STD) σ, the mean value of the STFT is equal to

$$\mathrm{E}\left\{\mathrm{STFT}_v\left(t_n, f_p\right)\right\} = \mathrm{STFT}_s\left(t_n, f_p\right), \quad (2)$$

where $v(t_n)=s(t_n)+\xi(t_n)$.

The STFT variance is

$$\mathrm{E}\left\{\left|\mathrm{STFT}_v\left(t_n, f_p\right) - \mathrm{STFT}_s\left(t_n, f_p\right)\right|^2\right\} = \sigma^2 \sum_k \left|w\left(t_k\right)\right|^2. \quad (3)$$

Therefore, noise characteristics in this case are neither signal, nor time and frequency dependent.

Situation with TFRs related to the noise influence becomes more difficult for nonlinear representations. For example, quite often instead of the complex-valued STFT its square magnitude version called spectrogram (SPEC) is considered:

$$\mathrm{SPEC}_s\left(t_n, f_p\right) = \left|\mathrm{STFT}_s\left(t_n, f_p\right)\right|^2. \quad (4)$$

The SPEC shares many favorable properties and weaknesses of the STFT but noise characteristics studied in depth in [11] are quite different. Namely, in the SPEC, the resulting noise is signal, time and frequency dependent. In the region of signal components, the noise variance is significantly higher than in the region where there are no signal components. Also, the resulting noise is not Gaussian but, in fact, it has Rayleigh pdf [22].

Considering nonlinear TFRs, the famous representation called the WD should be mentioned [23]. It was firstly introduced in the quantum mechanics and later on extended to the TF analysis and even became its cornerstone. WD is mainly used for improvement of the TF resolution. Namely, in the WD (here given in practical windowed-pseudo form), signal components are better concentrated and occupy significantly smaller part of the TF plane compared to the STFT or SPEC. The WD is defined as

$$\mathrm{WD}_s\left(t_n, f_p\right) = \sum_k s\left(t_n + t_k\right) s^*\left(t_n - t_k\right) w\left(t_k\right) \exp\left(-j2\pi f_p t_k\right), \quad (5)$$

The WD is real-valued TFR and its mean value for noisy signal is

$$\mathrm{E}\left\{\mathrm{WD}_v\left(t_n, f_p\right)\right\} = \sigma^2 \sum_k \left|w\left(t_k\right)\right|^2. \quad (6)$$

It is seen that WD mean value is non-zero but it is constant over entire TF plane and it does not influence TF image significantly nor other abilities of the TFRs in estimation, feature extraction, and detection. Variance of the WD is evaluated as

$$\mathrm{E}\left\{\left|\mathrm{WD}_v\left(t_n, f_p\right) - \mathrm{E}\left\{\mathrm{WD}_v\left(t_n, f_p\right)\right\}\right|^2\right\} = \sigma^2\left(2A^2 + \sigma^2\right) \sum_k \left|w\left(t_k\right)\right|^2, \quad (7)$$

under assumption that signal of interest is a mono-component FM $s(t_n) = A\exp(j\varphi(t_n))$, where $\varphi(t)$ is the total phase of the signal. Thus, the obtained noise is signal dependent. Here, for simplified FM signal model, the variance varies with changes of the signal amplitude but for other signal models it could be more complicated. In [23], it has been shown that the WD can be treated as Gaussian random fields [24].

The main difficulty associated with the WD is the fact that for signals with several components its TFR exhibits emphatic cross-terms. Therefore, numerous strategies were proposed for reducing the effect of interferences/cross-terms. Among them, there is an effective and simple TFR called the SM defined as [22]

$$\mathrm{SM}\left(t_n, f_p\right) = \int_{\theta} P(\theta)\,\mathrm{STFT}\left(t_n, f_p+\theta\right)\mathrm{STFT}^*\left(t_n, f_p-\theta\right)d\theta, \quad (8)$$

where $P(\theta)$ is a frequency domain low-pass filter.

For $P(\theta) = \pi\delta(\theta)$ we obtain the SPEC while for the $P(\theta)=1$ the WD follows. Selecting the filter as $P(\theta)=1$ for $\theta\in[-\phi; \phi]$ and $P(\theta)=0$ elsewhere for relatively small values of ϕ we can achieve significant concentration improvement without undesired terms and interferences.

Noise influence on the SM is partly studied in [15]. It has been shown that in the area of the SPEC auto-term the variance in the TF plane is higher while in the area where there are no signal components the variance is smaller. Note that the area of elevated variance does not correspond to small region of the SM highly concentrated auto-terms but too much wider region of the SPEC or STFT auto-terms. All other details required to understanding phenomena related to the noise influence on the TFRs (images) can be found in [25, 26].

Thus, one of the common ways to reduce noise influence on TFRs is to design or select the optimal transform for the corresponding signal and noise models. In this paper, we are going to demonstrate another way to cope with the noise influence in different TFRs. Namely, our idea is to apply advanced filtering methods [10, 19, 27] from image processing field at the post-processing stage of TFR. This can be done if we consider estimated TFR as an image. Following such an approach, the first step is to investigate noise characteristics at TFR image in order to choose a proper filter.

1.2. Resulting noise in SM

As it has been already mentioned, TFRs are noisy if disturbance is present in original signal. Such a situation can prevent solving further tasks of the TF analysis and processing. A possible direction for performance improvement is to remove noise by filtering while considering TFR as an image. There are numerous filters existing nowadays. To clarify what image denoising methods can be applicable for a particular case, it is necessary to specify noise model and its characteristics for data at hand. In order to do that for our task, consider a three-component test signal of the form

$$\begin{aligned} s(t_n) = {} & 0.7\exp\left(j36\pi t_n^2 - j12\pi t_n\right) + \\ & + 0.8\exp\left(j36\pi t_n^2 + j84\pi t_n\right) + \\ & + \exp\left(-j32\pi t_n^2 + j40\pi t_n\right), \end{aligned} \quad (9)$$

where $t_n=t_{st}+nT_S$,
t_{st}=-1 sec.,
$n\in[1; N]$,
N=512,
$T_S=T/N$,
T=2 sec.

The STFT is evaluated with window of the width 0.5 sec., while width of the frequency window in the SM is $\phi=24\pi$. This signal is used in all forthcoming examples and statistical analysis.

The SM of the test signal corrupted by an AWGN with the STD $\sigma=1$ is represented in Fig. 1a where signal components appear themselves as three inclined "strips" with noise clearly visible in homogeneous regions of this image. Note that the considered TFR has both positive and negative values. Such a situation differs from the case of traditional image processing where data usually have non-negative values.

The statistical characteristics of the resulting noise in the SM are studied in [15, 25]. For application of the filtering in the TFR domain here we will employ simulation and consider resulting noise behavior in the TF plane. For this purpose, we have obtained *M*=512 realizations of the SM and then analyzed statistics of each element (pixel) of the SM of the following form:

$$\Delta^{(m)}(t_n, f_p) = \mathrm{SM}^{(m)}(t_n, f_p) - \mathrm{SM}^{\mathrm{true}}(t_n, f_p), \quad (10)$$

where $m \in [1;M]$ is a realization index,
$\mathrm{SM}^{\mathrm{true}}(t_n, f_p)$ denotes the SM of noiseless signal.

While considering this task, we have been interested in finding answers to the following questions: 1) Is the noise induced in the SM Gaussian? 2) Is the noise spatially stationary (additive) or non-stationary (possibly, some kind of signal-dependent)? 3) Is the noise white or spatially correlated?

To answer the first question, different approaches can be applied. In particular, one can apply some Gaussianity tests [28]. It is also possible to use some parameters that characterize distribution tail heaviness [29]. These could be a standard kurtosis or its robust version called percentile coefficient of kurtosis (PCK) [28-30]:

$$\mathrm{PCK} = K_p = \frac{1}{2}\frac{Q_3 - Q_1}{P_{90} - P_{10}}, \quad (11)$$

where Q_1, Q_3, P_{90}, P_{10}, are the first and the third quartiles and the 90th and the 10th percentiles, respectively, of the sample to be analyzed.

Recall that, for Gaussian pdf the standard kurtosis is equal to 0 whilst it is larger for heavy-tailed distributions. Speaking of PCK values, they are close to 0.265 for data samples obeying Gaussian pdf and they are smaller than 0.265 for pdfs with heavier tails [30] (e.g., 0.21 for Laplacian distribution).

Analysis of standard kurtosis values of data $\Delta(t_n, f_p)$ (see Fig. 1b) shows that noise pdf is close to Gaussian for pixels that belong to "informative strips" whilst for other regions it is obviously non-Gaussian. Map of PCK values (see Fig. 1c) shows that noise characteristics are close to Laplacian in homogeneous regions and are almost Gaussian in places where signal components are present. Therefore, both tests are in good agreement and we can state that the resulting noise in the TFR is mainly heavy-tailed.

Due to non-Gaussian nature of the noise induced, it is worth analyzing robust estimates of noise intensity (scale). A popular technique to do this is to calculate the median of absolute deviations from the median (MAD) [28-30]:

$$\mathrm{MAD} = \mathrm{med}\left\{\left|x(t_n) - \mathrm{med}\left\{x(t_1),\ldots,x(t_N)\right\}\right|\right\}, \quad (12)$$

where $\mathrm{med}\{\ldots\}$ denotes the sample median,

$x(t_1),\ldots, x(t_N)$ are data values of the realization to be processed.

Analysis of data in Fig. 1d clearly shows that the resulting noise is non-stationary since such intensive spatial variations of MAD values cannot be explained by a limited sample size (M=512). Thus, the observed noise is of specific signal-dependent type having larger variance (scale) in places of signal component presentation. Besides, MAD for each pair of coordinates (n, p) has been found approximately proportional to the variance σ^2 of original data. Additional information on noise properties can be retrieved from the SM realization analysis. Histogram shown in Fig. 2 has been obtained by generating M=512 realizations of noisy signal (σ=1), calculating the SM (8) and processing M=512 samples of a pixel that belongs to a homogeneous fragment (with coordinates n=80 and p=80). Histogram from Fig. 3b has been obtained for manually selected quasi-

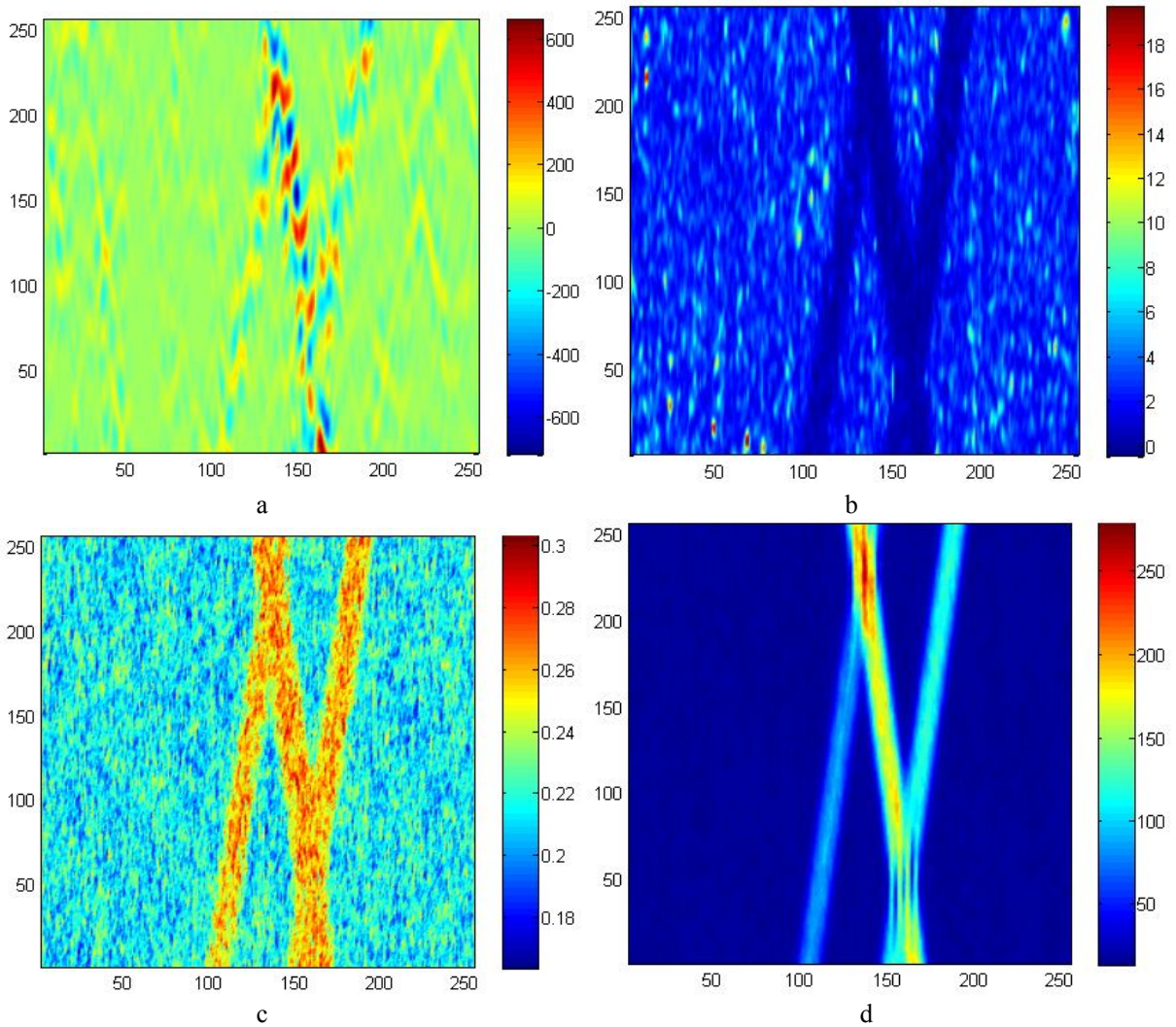

Fig. 1. Analysis of noise properties for the case of σ=1: one realization of TFR obtained by SM for noisy signal (9) (a), maps of statistical parameters: kurtosis (0 value corresponds to Gaussian process) (b), PCK (c) and MAD (d) values

homogeneous fragment of $SM^{(m)}(t_n, f_p)$ realization from Fig. 3a. In both cases, it is seen that distributions are not Gaussian and have heavy tails.

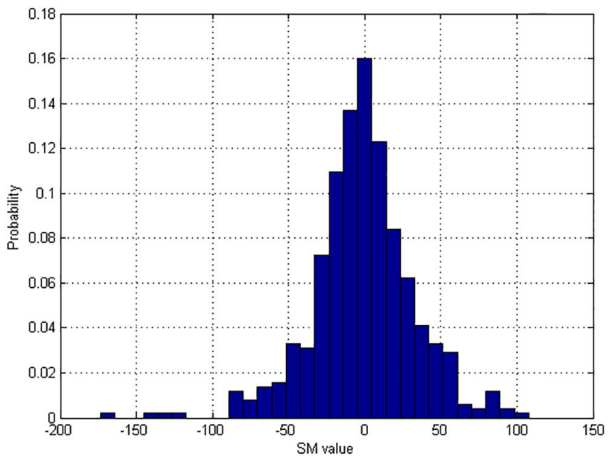

Fig. 2. Histogram of one pixel values (with coordinates n=80 and p=80)) in the SM for M=512 noisy realizations with σ=1

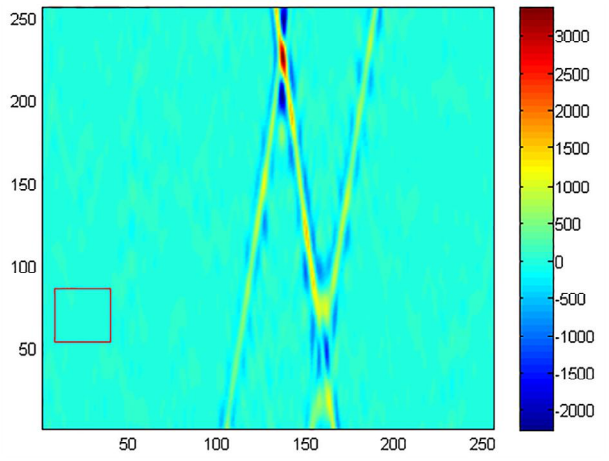

a

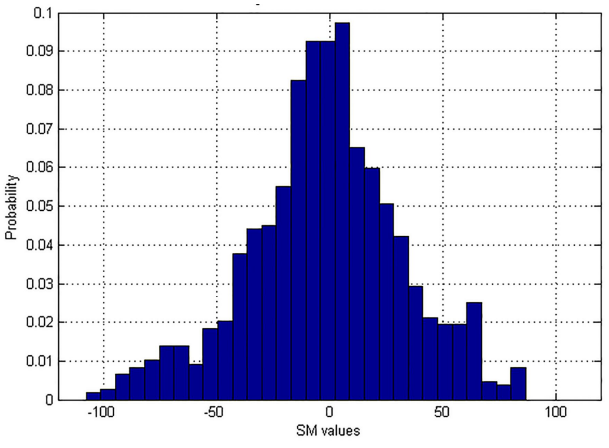

b

Fig. 3. $SM^{(m)}(t_n, f_p)$ estimate with manually selected quasi-homogeneous fragment of size 32x32 pixels (a) and histogram of $SM^{(m)}(t_n, f_p)$ values in the selected region (b)

In addition, an important characteristic of the resulting noise is its spatial correlation [31]. In order to check this property, we have obtained an estimate of 2-D auto-correlation function for manually selected quasi-homogeneous region marked in Fig. 3a. Fig. 4 represents this estimate in two different views.

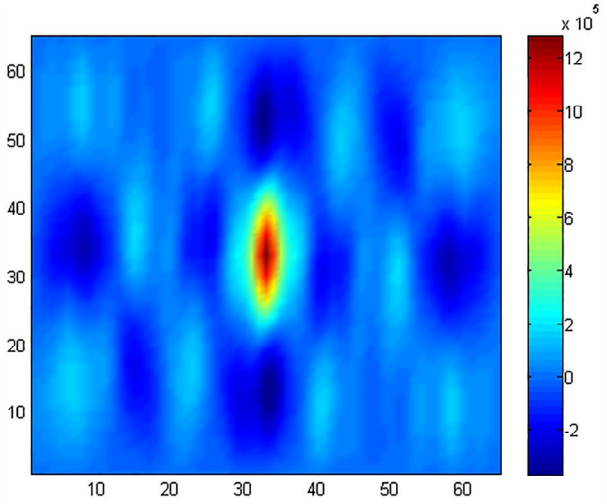

a

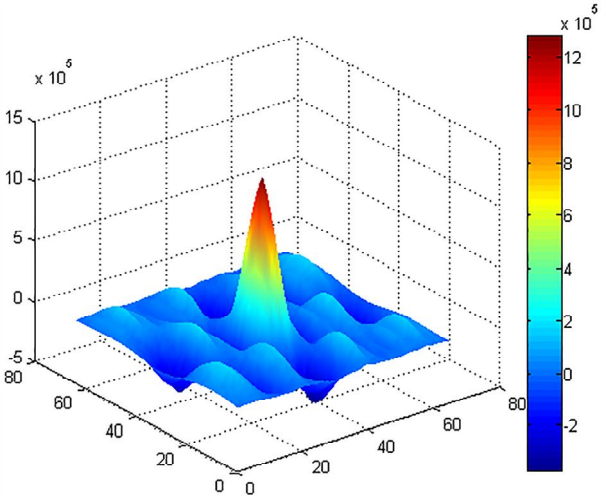

b

Fig. 4. Noise 2-D auto-correlation function estimate depicted by Matlab pcolor-function (a) and surf-function (b)

As it is seen, we can state that the noise is spatially correlated and correlation degree in one direction is larger than in another. These conclusions should be taken into account when choosing a proper filter for TFR processing.

2. Local and nonlocal filtering of SM

The observed practical situation is not typical for image denoising. Namely, there are numerous filters designed to cope with AWGN [27, 32, 33] where BM3D filter [10] is often considered to be state-of-the-art. Another group of filters has been proposed to cope

with such types of noise as speckle or Poisson [34, 35] or others [36, 37]. Notable exceptions from the previous class are filters from [31, 38] that have been designed for a priori known dependence of noise intensity (variance) on local parameters (e.g., mean) and for assumption that noise is spatially correlated. Some filters can perform in non-Gaussian noise environment [34, 37], but not for disturbance with Laplacian pdf. In our case, dependence of noise local intensity is a priori unknown, i.e., we deal with non-stationary noise with spatial correlation.

A simple solution could be to use nonlinear non-adaptive filters such as median, α-trimmed mean, Wilcoxon, etc. They are able to cope well with heavy-tailed non-stationary noise [39]. However, the main problem here is selection of the proper filter type which will work well both for regions with non-Gaussian interference and areas with Gaussian intensive noise.

2.1. Locally adaptive filters (LAF)

Possible solution for the considered problem are spatial adaptive filters. Locally adaptive robust filters are well tuned to the described situation [40, 41]. Such filters include, at least, a noise suppressing filter (NSF), a detail preserving filter (DPF) and a local activity indicator (LAI). The working algorithm of such filters is to calculate LAI (for a current position of sliding window) as the first step, then to compare the LAI value to some threshold and, finally, to make a decision what filter (NSF or DPF) to apply for evaluating output value for a given pixel. For the SM, application of LAF can be written as:

$$\mathrm{SM}^{\mathrm{LAF}}(t_n, f_p) = \begin{cases} \mathrm{SM}^{\mathrm{NSF}}(t_n, f_p), & \text{if } \mathrm{LAI}(t_n, f_p) \le \mathrm{TH}; \\ \mathrm{SM}^{\mathrm{DPF}}(t_n, f_p), & \text{if } \mathrm{LAI}(t_n, f_p) > \mathrm{TH}; \end{cases} \quad (13)$$

where $\mathrm{SM}^{\mathrm{NSF}}(t_n, f_p)$ and $\mathrm{SM}^{\mathrm{DPF}}(t_n, f_p)$ are NSF and DPF outputs, respectively,

TH denotes LAF threshold value.

The main idea of applying this kind of filters is that in our data (SM) we have locally passive (quasi-homogeneous) and locally active (strips and their edges) areas. Then, it is reasonable to apply NSF in locally passive areas and DPF for strips and their neighborhoods assuming that LAI allows discriminating them. Practical questions that arise for this group of filters are the following: what NSF and DPF to use? What should be a proper LAI and threshold for it for the considered application?

In order to find the answers, suppose that we know a priori or are able to accurately estimate σ in original noisy 1-D signal (9). Then, we check dependence of the noise statistics in quasi-homogeneous regions with respect to σ. For this purpose, histograms of SM values for single pixel with coordinates (n, m)=(80, 80) have been obtained for four values of σ (see Fig. 5). It is seen that histogram shapes remain practically the same (distribution close to the Laplacian) but data scale quickly grows with increasing of σ. Data provided actually characterize the STD in quasi-homogeneous regions of the SM.

To confirm numerically the conclusion made on the basis of the histograms' shape, the STD of the pixel values (σ_{IND}) are presented in Table 1 for considered four input noise σ values. The obtained data show that σ_{IND} values are approximately proportional to σ^2. We can adopt an approximation expression between input noise STD σ value and induced noise STD σ_{IND} as

$$\sigma_{\mathrm{IND}} = 35\sigma^2. \quad (14)$$

Its values provided in the second row of the Table 1 show that the expression is good enough. Note that the approximation is valid only for the considered size of input signal and Gaussian noise affecting the signal. It also depends upon window function used. However, the main idea is that in each particular situation the proportionality factor can be determined in advance.

The resulting noise scale in quasi-homogeneous region can be also characterized in another way. It can be observed from analysis of data in Fig. 1d that parameter MAD (12) values are almost constant in homogeneous regions.

Therefore, it is possible to determine local MAD for 7x7 scanning window as

$$\mathrm{MAD}(t_n, f_p) = \mathrm{med}\left\{\left|\mathrm{SM}(t_i, f_j) - \mathrm{med}\left\{\mathrm{SM}(t_i, f_j)\right\}\right|, \right. \quad (15)$$
$$\left. i = n-3, \ldots, n+3,\ j = p-3, \ldots, p+3\right\}.$$

Table 1

Dependence of induced noise STD on input noise STD

	Input noise STD, σ			
	0.1	0.5	1	1.5
Induced noise STD, σ_{IND}	0.35	9.32	33.61	90.15
$\sigma_{\mathrm{IND}}^{\mathrm{APPR}} = 35\sigma^2$	0.35	8.75	35	78.75

Histograms of local MAD estimates calculated in fully overlapping blocks of 7x7 pixel size are presented in Fig. 6 for two values of input noise STD. As it is seen, local MAD estimates are mostly smaller than value calculated according to approximation formula (14). Such local estimates mostly relate to quasi-homogeneous regions whilst there are also local estimates with considerably larger values corresponding to signal component area. Thus, we can use the value $35\sigma^2$ as the LAF threshold value TH in (13) for discriminat-

ing the locally passive and active areas in SM image. i.e. if the local MAD value in current block is less or approximately equal to 35 σ^2 then we most probably are in quasi-homogeneous region of TFR and NSF should be applied, and vice versa.

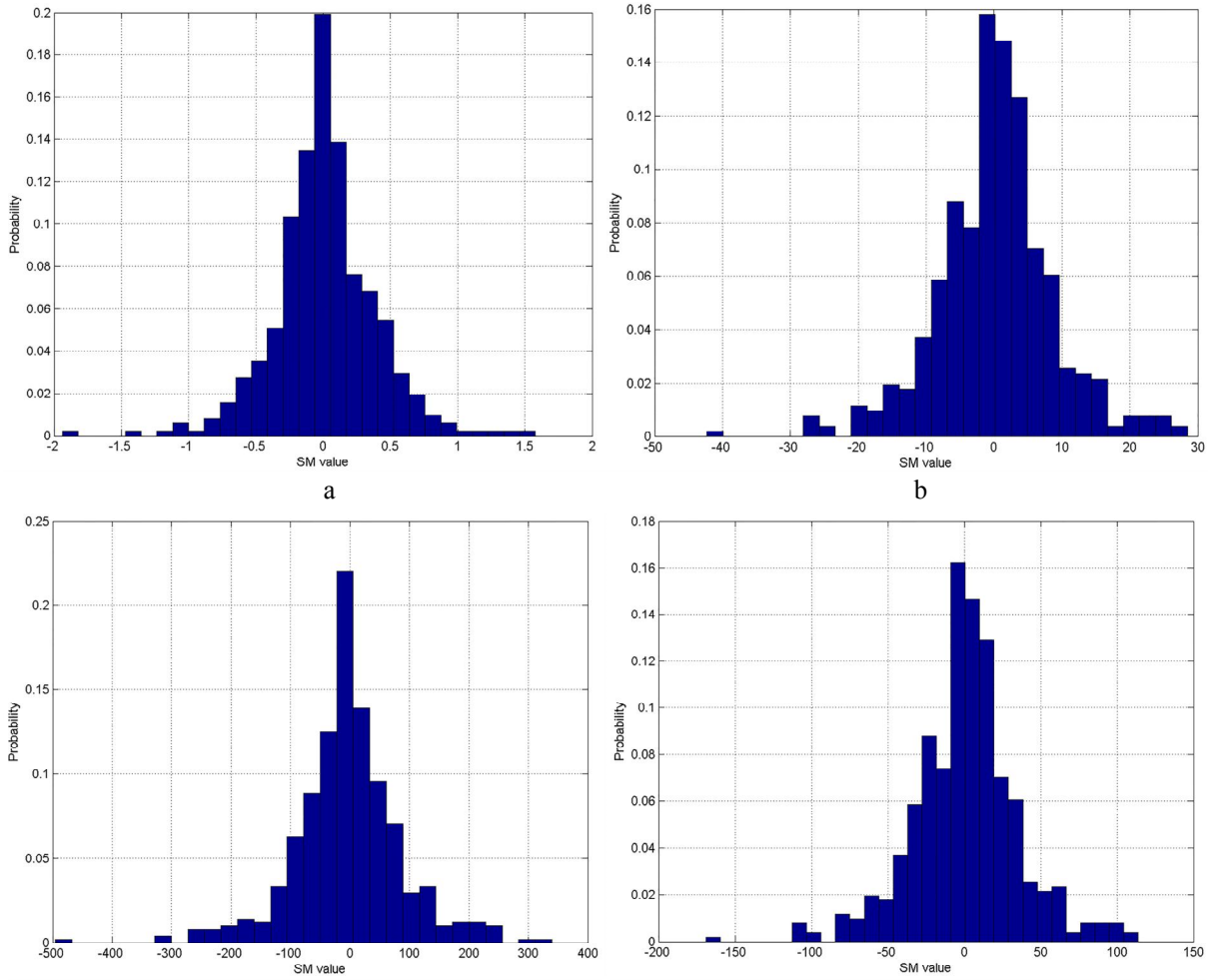

Fig. 5. Histograms of $SM^{(m)}(t_n, f_p)$ values for n=80 and p=80 for σ=0.1 (a), σ=0.5 (b), σ=1.0 (c), σ=1.5 (d)

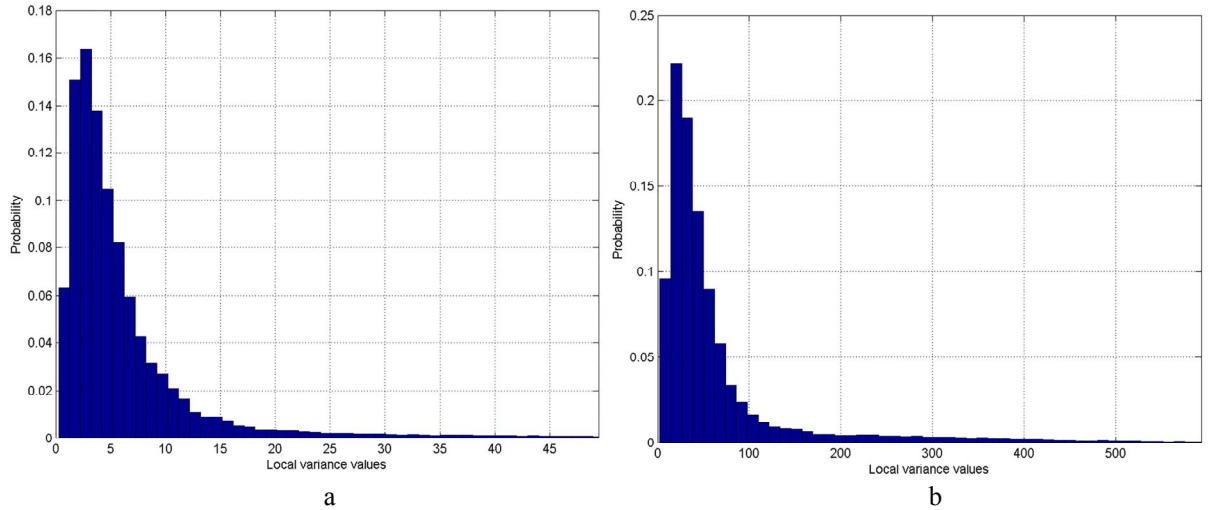

Fig. 6. Histograms of local MAD estimates calculated in fully overlapping blocks of 7x7 pixel size for input noise STD values σ=0.5 (a) and σ=1.5 (b)

2.2. Orthogonal transform based image filters

There are also other options to filter TFRs. One of them described in [42] uses wavelet-based denoising algorithm whilst the approach considered in [43] implements bilateral filtering. In both cases, it is demonstrated that denoising of TFRs leads to certain improvement but no quantitative data are presented.

Certain degree of adaptation to noise local intensity and image content can be done applying locally adaptive DCT-based filters [44]. The general principles of DCT-based denoising are the following. It is carried out in blocks of 8x8 pixels (the most typical size). In each block, 2-D DCT is calculated and the obtained DCT coefficients are compared to one or several thresholds. If noise is approximate white, the threshold is set fixed for all DCT coefficients for a given block position (thresholds can be frequency dependent if noise is spatially correlated and its DCT spectrum is a priori known or pre-estimated). Meanwhile, if noise is not stationary, different thresholds can be set for different positions of blocks. In particular, a typical practice is to set threshold(s) proportional to local noise STD (or its estimate obtained in one or another manner [42]).

The next operation performed in each block is thresholding. Similarly to wavelet denoising techniques, there are several types of thresholding schemes but one of the most efficient and simple is hard thresholding. It will be used in DCT-based TFR denoising filter as:

$$D_{SM}^{thr}\left(k,l,t_n,f_p\right) = \begin{cases} D_{SM}\left(k,l,t_n,f_p\right), \text{ if } \left|D_{SM}\left(k,l,t_n,f_p\right)\right| \geq T\left(k,l,t_n,f_p\right); \\ 0, \text{ otherwise;} \end{cases} \quad (16)$$

where $D_{SM}\left(k,l,t_n,f_p\right)$ is the kl-th DCT coefficient in the considered block,

$T\left(k,l,t_n,f_p\right)$ denotes a threshold value, block position is determined by its left upper corner (indices of t_n and f_p),

$D_{SM}^{thr}\left(k,l,t_n,f_p\right)$ is the kl-th DCT coefficient in the considered block after thresholding operation.

Then, inverse 2-D DCT is applied to the thresholded DCT coefficients and filtered values of processed data (image) are obtained for all pixels belonging to a given block. Note that blocks can be non-overlapping, partly overlapping, and fully overlapping. In the latter two cases, the filtered values for a given pixel are averaged for all blocks this pixel belongs to. Full overlapping requires more computations than denoising in partly or non-overlapping blocks but it usually gives smaller output mean square error (MSE).

A problem that can arise is that the DCT-based filters in [44] have not been tried for spatially correlated and heavy-tailed noise. This is an obstacle that can cause problems [31, 45, 46], and restrict performance of such filters. Another problem deals with local adaptation mechanisms proposed in [44]. They relate to local estimation of noise standard deviation (denoted as $\hat{\sigma}\left(k,l,t_n,f_p\right)$ in our case) and to local adaptation of proportionality factor $\beta\left(t_n,f_p\right)$ used in threshold setting as $T\left(k,l,t_n,f_p\right)=\beta\left(t_n,f_p\right)\cdot\hat{\sigma}\left(k,l,t_n,f_p\right)$. These aspects should be carefully checked in future experiments. In our studies, we have considered a fixed threshold.

2.3. Non-local filters

Finally, there are numerous non-local filters proposed recently [10, 27]. Their peculiarity is that they employ search of similar patches and joint processing of data for each formed set of such patches. To our best knowledge, nonlocal filtering techniques have not been tried for denoising data (images) with noise properties described previously. An obvious problem is that both search and joint processing have to be adapted to noise. Therefore, we have decided to consider application of the BM3D filter [10] to our data.

The BM3D has elaborated algorithm realization with selection of the similar patches. These patches are put into 3D array and they are filtered together using 3D linear transform. In this way similar patches in images are filtered together and this allows using important property of these nonlocal patches that correlation between noises is smaller than of patch signal components. This algorithm is proposed in [10]. Detailed analysis of realization is provided in [20, 47]. Here only very brief algorithm realization will be provided while for all other details for interested readers the program realization can be found in [48].Rough filtering stage consists of search for similar (commonly rectangular patches), forming 3D matrix of these patches, calculation of the 3-D discrete linear transform (commonly DCT or Hadamard/Walsh) and filtering using hard threshold technique (transform coefficients below threshold are set to 0). In the fine filtering stage again similar blocks (patches) are found forming 3D array followed by evaluation of the 2D discrete linear transform. Now, filtering is performed in the transform domain using Wiener filter. The same pixel in the image can belong to various filtered blocks and final output is obtained using aggregation of results with different blocks.

The TFRs have large areas influenced by noise. These areas represent similar patches that can be efficiently filtered with both local and nonlocal filters. In

addition, similar patches (blocks) can be recognized in the TF plane in area of the signal components. Then application of nonlocal filtering to these parches is supposed to improve filtering of the TFR.

The available versions of BM3D filter can only be applied to data having non-negative values. Then it is necessary to provide certain pre-processing stage which includes finding the minimal value of current realization of TFR denoted as SM_{min}, and using its absolute value to shift the TFR data for obtaining a realization array of non-negative values. After that, the BM3D is used and results in preliminary filtered data $SM_{filt}^{prel}\left(t_n, f_p\right)$. Then, the determined shift value, $|SM_{min}|$, is subtracted from $SM_{filt}^{prel}\left(t_n, f_p\right)$ for obtaining final processed data array $SM^{BM3D}\left(t_n, f_p\right)$.

A key question here is that in order to perform the BM3D filtering, noise STD in a filtered process should be known or pre-estimated in advance. In Section 5.3, we propose methodology to solve this practical question. We understand that such a discrepancy between actual and assumed noise properties can lead to reduced filtering efficiency. Meanwhile, we expect that certain positive effect from such denoising can be achieved in any case.

3. Performance criterions used

Therefore, we have the practical situation which is very rarely met in practice with respect to image (TFR) subject to filtering. Note that assessment of denoising efficiency for the considered application is specific as well. We need such a denoising that should be able to suppress noise in quasi-homogeneous regions without introducing distortions into informative fragments that correspond to signal components. Besides, we deal with non-Gaussian noise in data where MSE is not the best criterion to characterize filtering efficiency.

To take into account these peculiarities, the following criteria have been used in further studies. First, output MSE which is the well-known and often applied parameter was employed. We calculated MSE for entire TFR (MSE_{INT}) and for pixels belonged to the signal components only (MSE_{SC}):

$$MSE_{INT} = \frac{1}{N \cdot P} \sum_{n=1}^{N} \sum_{p=1}^{P} \left\{ \frac{1}{M-1} \cdot \sum_{m=1}^{M} \left[TFR_{FILT}^{(m)}\left(t_n, f_p\right) - \overline{TFR}_{FILT}\left(t_n, f_p\right) \right]^2 \right\}, \quad (17)$$

$$MSE_{SC} = \frac{1}{N_{SR} \cdot P_{SR}} \sum_{n \in N_s} \sum_{p \in P_s} \left\{ \frac{1}{M-1} \cdot \sum_{m=1}^{M} \left[TFR_{FILT}^{(m)}\left(t_n, f_p\right) - \overline{TFR}_{FILT}\left(t_n, f_p\right) \right]^2 \right\}, \quad (18)$$

where $TFR_{FILT}^{(m)}\left(t_n, f_p\right)$ denotes the value of a pixel with coordinates (t_n, f_p) for the m-th realization of filtered TFR,

$\overline{TFR}_{FILT}\left(t_n, f_p\right)$ denotes averaged (over the ensemble of M=32 realizations) value for the same pixel with coordinates (t_n, f_p),

N_S and Ω_S are the sets of indices of the signal component region,

N_{SR} and Ω_{SR} denote the total number of pixels in the signal component region.

Besides, we were also interested in mean absolute error (MAE) calculated with respect to noise-free SM [39]. The MAE is also evaluated for entire SM (MAE_{INT}) and for regions of signal component only (MAE_{SC}):

$$MAE_{INT} = \frac{1}{N \cdot P \cdot M} \cdot \sum_{n=1}^{N} \sum_{p=1}^{P} \sum_{m=1}^{M} \left| TFR_{FILT}^{(m)}\left(t_n, f_p\right) - \overline{TFR}_{FILT}\left(t_n, f_p\right) \right|; \quad (19)$$

$$MAE_{SC} = \frac{1}{N_{SR} \cdot P_{SR} \cdot M} \cdot \sum_{n \in N_s} \sum_{p \in P_s} \sum_{m=1}^{M} \left| TFR_{FILT}^{(m)}\left(t_n, f_p\right) - \overline{TFR}_{FILT}\left(t_n, f_p\right) \right|. \quad (20)$$

The input MSE has been calculated as well:

$$MSE_{INT} = \frac{1}{N \cdot P} \sum_{n=1}^{N} \sum_{p=1}^{P} \left\{ \frac{1}{M-1} \cdot \sum_{m=1}^{M} \left[TFR_{NOISY}^{(m)}\left(t_n, f_p\right) - TFR_{NF}\left(t_n, f_p\right) \right]^2 \right\}, \quad (21)$$

where $TFR_{NOISY}^{(m)}\left(t_n, f_p\right)$ is the m-th realization of noisy TRF,

$TFR_{NF}^{(m)}\left(t_n, f_p\right)$ is a noise-free TFR.

MSE_{INT} should be considerably smaller than MSE_{INP} and it is possible to characterize filtering efficiency by the ratio MSE_{INT}/MSE_{INP} (the smaller, the better). Similarly, it is possible to determine input MAE. The ratio of output MAE to input MAE should be as small as possible as well.

There is also one more requirement to the denoising methods under study. We would like them to be efficient for a wide range of input signal-to-noise ratios (SNR). Therefore, the study has been carried out for variations in input SNR value from 6.8 to 0.8. To simu-

late such a variation, four different values of input noise STD σ have been used in experiments, namely, 0.5, 0.7, 1, and 1.5.

4. Analysis of obtained results

4.1. Local nonlinear filters

As the simplest representative of non-adaptive nonlinear filters, the median filter with two different window sizes, namely, 3x3 and 5x5 pixels, has been analyzed. The results are presented in Tables 2-5. As it is seen from Table 2, MSE_{INP} grows faster than proportionally to σ^2, whilst input MAE grows faster than proportionally to σ (see data in Table 4). Median 3x3 filter leads to output MSE values smaller in comparison to MSE_{INP} but this reduction is not large (see data in Tables 2 and 3). This takes place for all considered σ. Output MAE is approximately of the same order as input MAE (see data in Tables 4 and 5). Thus, there is no obvious benefit in applying the 3x3 median filter.

Table 2

Output MSE calculated for entire TFR

		Input noise STD, σ			
		0.5	0.7	1	1.5
Input MSE		1373	3045	6658	18446
		Output MSE (MSE_{INT})			
Output MSE	Median (3x3)	1282	2814	6055	16508
	Median (5x5)	1036	2218	4686	12490
	LAF1	1338	2928	6203	16222
	LAF2	1328	2874	5965	15285

Table 3

Output MSE calculated for signal component area

		Input noise STD, σ			
		0.5	0.7	1	1.5
Input MSE		9792	20973	41280	93020
		Output MSE (MSE_{SC})			
Output MSE	Median (3x3)	9276	19694	38229	84840
	Median (5x5)	7617	15757	30119	65181
	LAF1	9704	20773	40832	92292
	LAF2	9704	20781	41267	96523

As to the local MSE_{SC} values, the 5x5 median filter performs rather well (see data in Table 3), whilst according to MAE_{INT} criterion, the results are not good. They are in three out of four cases larger than input MAE values for entire TFR (see data in Table 4). The most undesirable fact is that output MAE for this filter can be sufficiently larger than input MAE for signal component area (Table 5).

Table 4

Output MAE calculated for entire TFR

		Input noise STD, σ			
		0.5	0.7	1	1.5
Input MAE		16.8	27.0	44.8	84.4
		Output MAE (MAE_{INT})			
Output MAE	Median (3x3)	17.7	26.8	43.4	80.3
	Median (5x5)	24.5	31.2	44.8	75.5
	LAF1	15.6	24.5	39.6	72.4
	LAF2	15.3	23.8	38.1	69.2

A larger size median filter (5x5 pixel scanning window) is known to suppress noise better but by the expense of worse preservation of important details and edges in some cases. This statement is proved by data in Table 2 where output MSE_{INT} values show that results for 5x5 median filter are better in comparison to the case of 3x3 median filter.

Table 5

Output MAE calculated for signal component area

		Input noise STD, σ			
		0.5	0.7	1	1.5
Input MAE		77.2	111.8	155.5	234.5
		Output MAE (MAE_{SC})			
Output MAE	Median (3x3)	89.6	118.1	158.7	230.8
	Median (5x5)	154.7	169.8	197.8	249.2
	LAF1	77.1	111.3	154.8	234.1
	LAF2	77.1	111.3	155.9	243.4

4.2. Locally adaptive nonlinear filters

We have analyzed two variants of LAFs denoted as LAF1 and LAF2. In LAF1, as noise suppression filter (NSF) we propose to apply 7x7 pixel α-trimmed mean filter with outer trimming parameter equal to 10% (i.e., 5 largest and 5 smallest values in ordered data sample in a given scanning window are rejected before averaging the remainder values). Larger 7x7 scanning window is motivated by necessity to efficiently suppress spatially correlated noise with remaining mean for pdfs that are symmetric with respect to location parameter [37, 43]. As the DPF, we propose 3x3 center weighted median filter (CWMF) [39] with rather large weight (value 5 is adopted in our experiments). Such a filter removes spikes but keeps almost all other values unchanged. Clearly, noise suppression efficiency of this filter is not high but it practically does not destroy information content. Local MAD value (scale characteristic) is used as a local activity indicator and a threshold value depending on induced noise STD σ_{IND}. The threshold is set equal to $35\ \sigma^2$.

According to output MSE values (integral in Table 2 and local in Table 3), LAF1 provides approximately the same results as the 3x3 median filter and worse than 5x5 median filter. However, according to MAE criterions (integral in Table 4 and local in Table 5), the use of LAF1 leads to slightly better results than for the analyzed standard median filters.

The locally adaptive filter LAF2 differs from LAF1 by the set threshold only which is equal to 70 σ^2 for LAF2. This does not change the results considerably – a slightly better noise suppression in homogeneous regions is provided (smaller values of integral MSE in Table 2 and integral MAE in Table 4) by the expense of a little bit worse processing in signal component area (greater values of local MSE in Table 3 and local MAE in Table 5).

Concluding our analysis for non-adaptive and adaptive nonlinear filters, we can state that some noise reduction with useful information preservation can be achieved but the benefit is not large. Maybe, other NSFs, DPFs, LAIs or different thresholds can produce better results.

4.3. DCT filter

The next considered solution for the SM denoising is the application of locally adaptive DCT-based filter [44]. If noise is white and additive, a general recommendation is to set the filter threshold as $T = \beta\hat{\sigma} \approx 2.6\hat{\sigma}$ where $\hat{\sigma}$ is the estimate of noise STD. If noise is spatially correlated and we do not adapt to noise spectrum, optimal β that provides the best noise suppression efficiency can be considerably larger than 2.6 [45]. Therefore, we apply different threshold values T for analyzing its influence on the performance of the DCT-based filter for the considered application. The obtained results are presented in Tables 6-9.

Analysis of integral MSE (Table 6) shows that the increase of T results in reduction of MSE_{INT} without reaching minimum for the considered range of the threshold variations. It can be explained by the following fact. Quasi-homogeneous regions occupy large part of TFR and noise suppression ability of applied filter has the main impact on the estimated output MSE_{INT}. Since the increase of threshold value leads to better suppression of spatially correlated noise [45], steady decreasing of output MSE_{INT} is observed.

Reduction is not large but for intensive input noise the output MSE_{INT} can be about 1.7 times smaller than input integral MSE value. Larger threshold leads to smaller local MSE (Table 7). However, optimum is not reached although threshold value is varied in wide limits. The situation changes if MAE criterion is analyzed. According to data in Table 8, optimum (minimum MAE value) is observed if $T \approx 20\hat{\sigma}$ where $\hat{\sigma}$ is defined as $\hat{\sigma} = \sigma_{IND}^{APPR} = 35\sigma^2$. According to Table 9, optimum takes place for slightly smaller T. We have considered cases ($T \approx 20\hat{\sigma}$ and $T \approx 10\hat{\sigma}$) of adaptive choice of T value. Obtained results are presented in two lowest rows of Tables 6-9. As it is seen, positive effect takes place according to all analyzed criteria but this effect is not too large.

Table 6

Output MSE calculated for entire TFR

			Input noise STD, σ			
			0.5	0.7	1	1.5
Input MSE			1373	3045	6658	18446
			Output MSE (MSE_{INT})			
DCT filter modifications	**Threshold value T**	5	1372	3044	6656	18443
		50	1335	2976	6555	18311
		100	1307	2893	6369	18007
		200	1272	2786	6028	17171
		400	1220	2660	5572	15479
		800	1125	2453	5036	13089
		1600	1050	2255	4537	10963
		1800	1032	2205	4417	10616
		$10\sigma_{IND}^{APPR}$	1313	2811	5664	13146
		$20\sigma_{IND}^{APPR}$	1280	2691	5144	11008

Table 7

Output MSE calculated for signal component area

			Input noise STD, σ			
			0.5	0.7	1	1.5
Input MSE			9792	20973	41280	93020
			Output MSE (MSE_{SC})			
DCT filter modifications	**Threshold value T**	5	9792	20972	41279	93018
		50	9772	20937	41222	92917
		100	9738	20872	41107	92693
		200	9636	20714	40826	92118
		400	9396	20223	39887	90179
		800	8769	18900	37160	84022
		1600	8206	17408	33630	73415
		1800	8038	16969	32645	70980
		$10\sigma_{IND}^{APPR}$	9748	20766	40160	84234
		$20\sigma_{IND}^{APPR}$	9667	20370	37829	73718

4.4. BM3D filter

It has been mentioned above that for operation of BM3D filter one needs to set the noise STD value. There is no such a priori information for the considered application but it is possible to use formula (14), i.e. $\sigma_{IND}^{APPR} = 35\sigma^2$, as some "most often met" standard deviation or to employ other values. Results obtained for wide range of a priori set induced noise STD values (for

filter application) as well as for value σ_{IND}^{APPR} and 2 and 3 times larger than σ_{IND}^{APPR} are given in Tables 10-13.

Table 8

Output MAE calculated for entire TFR

			Input noise STD, σ			
			0.5	0.7	1	1.5
Input MAE			16.8	27.1	44.8	84.4
			Output MAE (MAE_{INT})			
DCT filter modifications	**Threshold value T**	5	16.8	27.1	44.8	84.4
		50	15.1	25.3	43.5	83.7
		100	14.4	23.6	41.3	82.1
		200	14.1	22.1	37.8	77.6
		400	14.1	21.4	34.5	69.7
		800	15.3	21.8	33.2	61.3
		1600	21.6	26.3	36.1	58.7
		1800	23.9	28.1	37.2	59.1
		$10\sigma_{IND}^{APPR}$	14.5	22.3	35.1	61.5
		$20\sigma_{IND}^{APPR}$	14.1	21.4	33.3	58.7

Table 9

Output MAE calculated for signal component area

			Input noise STD, σ			
			0.5	0.7	1	1.5
Input MAE			77.2	111.8	155.5	234.5
			Output MAE (MAE_{SC})			
DCT filter modifications	**Threshold value T**	5	77.2	111.8	155.5	234.5
		50	77.1	111.7	155.3	234.3
		100	77.1	111.5	155.1	234.1
		200	76.9	111.1	154.6	233.4
		400	77.8	110.6	153.4	231.3
		800	86.4	114.1	153.4	226.9
		1600	131.5	145.5	174.5	231.9
		1800	148.8	158.7	183.9	236.1
		$10\sigma_{IND}^{APPR}$	77.1	111.3	153.7	227.1
		$20\sigma_{IND}^{APPR}$	76.9	110.7	152.9	231.5

Interestingly, when filter parameter increases, the output MSE_{INT} almost steadily decreases (Table 10). Output MSE_{INT} can be up to 4…5 smaller than input MSE value, i.e. filtering is rather efficient according to the considered criterion. It seems possible to set the filter parameter as high as $105\sigma^2$ (the lower row of Table 10). Analysis of output MSE_{SC} (Table 11) leads to similar conclusions. There is a tendency to local MSE decreasing if the filter parameter increases.

According to local MAE criterion (Table 13), setting the BM3D parameter equal to $35\sigma^2$ can be a good practical choice. Compared to the DCT-based filter with the best parameters settings, there is benefit of about 10% in denoising of signal component area and substantial improvement in noise suppression efficiency in quasi-homogeneous regions. For visual comparison the SM estimates obtained by the investigated filtering methods are represented in Figs. 7-11.

Table 10

Output MSE calculated for entire TFR

			Input noise STD, σ			
			0.5	0.7	1	1.5
Input MSE			1373	3045	6658	18446
			Output MAE (MSE_{INT})			
BM3D modifications	**BM3D Parameter**	5	1118	2611	5864	16786
		50	602	1455	3256	9374
		100	567	1338	2876	7587
		200	471	1175	2562	6205
		400	296	711	1670	4487
		600	307	715	1598	4112
		$35\sigma^2$	978	2024	3915	8145
		$70\sigma^2$	824	1768	3016	6690
		$105\sigma^2$	766	1446	2869	5805

Table 11

Output MSE calculated for signal components' area

			Input noise STD, σ			
			0.5	0.7	1	1.5
Input MSE			9792	20973	41280	93020
			Output MSE (MSE_{SC})			
BM3D modifications	**BM3D Parameter**	5	8636	19437	39329	90300
		50	4827	11480	24293	59646
		100	4526	10523	21517	49776
		200	3662	9031	18812	39893
		400	2085	4900	10833	25258
		600	2013	4539	9334	20522
		$35\sigma^2$	7684	15682	28589	53123
		$70\sigma^2$	6532	13739	22528	43656
		$105\sigma^2$	6075	11405	21466	36678

Table 12

Output MAE calculated for entire TFR

			Input noise STD, σ			
			0.5	0.7	1	1.5
Input MAE			16.8	27.0	44.8	84.4
			Output MAE (MAE_{INT})			
BM3D modifications	**BM3D Parameter**	5	13.1	22.1	38.6	77.3
		50	15.4	19.7	29.3	55.1
		100	23.1	26.2	33.8	54.1
		200	40.7	42.1	47.1	61.4
		400	68.3	68.6	69.5	76.3
		600	99.4	99.7	99.2	99.8
		$35\sigma^2$	12.3	19.1	31.2	53.6
		$70\sigma^2$	12.1	19.8	30.7	58.1
		$105\sigma^2$	12.8	19.9	34.5	64.1

Table 13

Output MAE calculated for signal components' area

			Input noise STD, σ			
			0.5	0.7	1	1.5
Input MAE			77.2	111.8	155.5	234.5
			Output MAE (MAE_{SC})			
BM3D modifications	**BM3D Parameter**	5	72.1	106.8	151.1	230.6
		50	94.4	109.9	140.6	204.6
		100	146.5	154.2	175.7	223.9
		200	257.1	257.7	266.4	285.6
		400	331.5	332.6	334.1	339.4
		600	333.9	336.2	338.4	348.4
		$35\sigma^2$	68.6	97.9	139.2	213.5
		$70\sigma^2$	67.8	102.9	151.8	261.1
		$105\sigma^2$	72.8	111.1	180.5	301.5

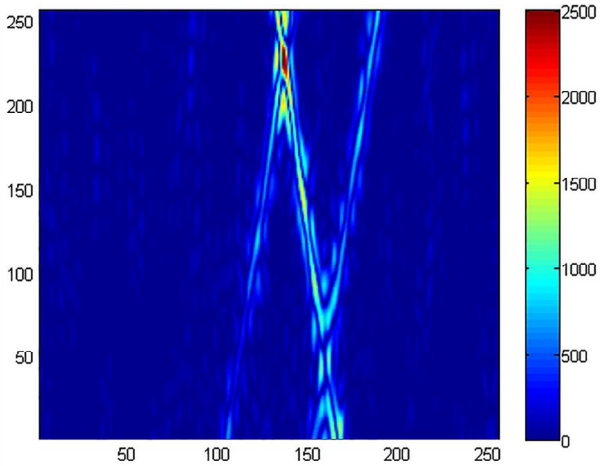

Fig. 7. SM realization at the input of filtering stage (MAE_{INT} = 44.1, MAE_{SC} = 158.6)

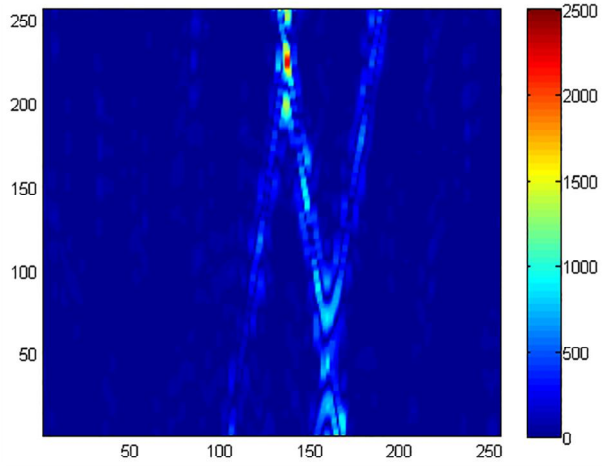

Fig. 8. SM estimate at the output of MED 5x5 filtering stage (MAE_{INT} = 44.5, MAE_{SC} = 202.7)

Alongside with the filtered TFRs (Figs. 8-11), we present integral and local MAE values for convenience of analysis. It is seen that processing based on median filtering in 5x5 sliding window size (Fig. 8) suppresses noise but at the same time introduces distortions to the signal components. Such results are not surprising and have been predicted. Filtering approach based on LAF2 (Fig. 9) performs better. Namely, there is smaller number of the undesired signal components with respect to the initial SM representation. Better filtering efficiency is observed for the DCT and BM3D filters (Figs. 10 and 11). Interferences between components are attenuated with respect to the previous filtering strategies but at the expense of significant damage of the weakest signal component.

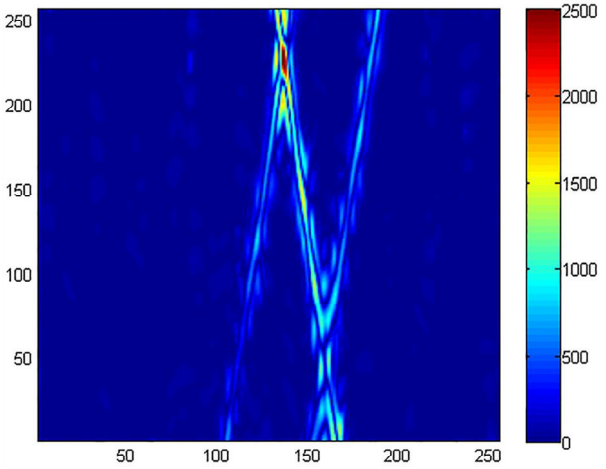

Fig. 9. SM estimate at the output of LAF2 (with $T=70\sigma^2$) filtering stage (MAE_{INT} = 37.6, MAE_{SC} = 159.1)

Comparison of SM estimates obtained by the DCT and BM3D filters shows that the BM3D preserves the most powerful signal component as well as the second signal component better than the DCT filter. This conclusion is also proved by MAE values (Tables 9 and 12).

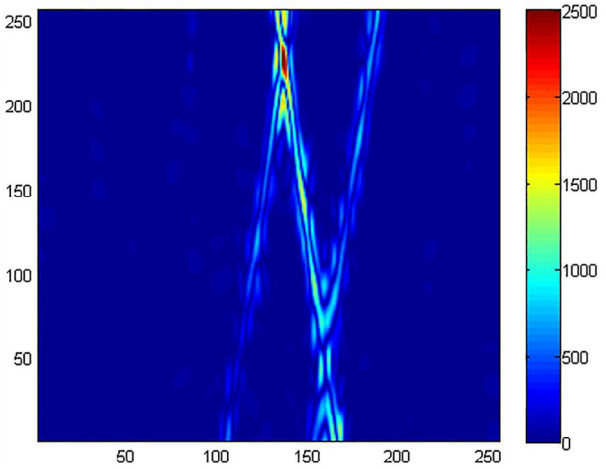

Fig. 10. SM estimate at the output of DCT1 (with T=600) filtering stage (MAE_{INT} = 33.9, MAE_{SC} = 158.9)

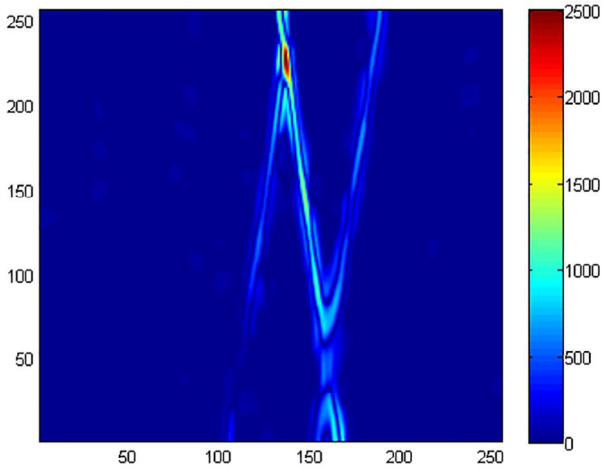

Fig. 11. SM estimate at the output of BM3D (with filter parameter $70\sigma^2$) filtering stage (MAE_{INT} = 32.1, MAE_{SC} = 164.7)

Conclusions

Filtering of S-method TFRs using filtering techniques common in the digital image processing has been studied. Even if the original 1-D signal is corrupted by AWGN, the noise induced in the S-method occurs to be the non-Gaussian, signal-dependent and spatially correlated. This makes the task of the S-method denoising quite complex.

Several approaches to noise suppression are studied. They include local nonlinear non-adaptive and adaptive techniques, orthogonal transform based filtering (namely, DCT-filter) and nonlocal processing approach based on the block matching 3-D filter. Considered filtering techniques are compared using the standard MSE and MAE metrics determined for both entire TFR and a part of TFR containing signal components only.

Analysis shows that significant enhancement (denoising effect) can be achieved but it is difficult to provide a trade-off for such filter properties as noise suppression quality and detail preserving performance. At the moment, the best results have been obtained by the BM3D filter for which input parameter has been adapted to noise properties in a simple way. We are confident that better results can be obtained in future if spatial correlation of noise is taken into consideration.

References (GOST 7.1:2006)

1. Gröchenig, K. Foundations of Time-Frequency Analysis [Text] / K. Gröchenig. – Boston : Birkhäuser, 2001. – P. 30-40.

2. Sejdić, E. Time-frequency feature representation using energy concentration: An overview of recent advances [Text] / E. Sejdić, I. Djurović, J. Jiang // Digital Signal Processing. – Jan. 2009. – vol. 19, no. 1. – P. 153-183.

3. Papandreou-Suppappola, A. Applications in Time-Frequency Signal Processing [Text] / A. Papandreou-Suppappola. – CRC Press, 2002. – 432 p.

4. Jones, D. L. A high resolution data-adaptive time-frequency representation [Text] / D. L. Jones, T. W. Parks // IEEE Trans. on ASSP. – Dec. 1990. – Vol. 38, No. 12. – P. 2127-2135.

5. Amin, M. G. Minimum-variance time-frequency distribution kernels for signals in additive noise [Text] / M. G. Amin // IEEE Trans. Signal Processing. – Sept. 1996. – Vol. 44, No. 9. – P. 2352–2356.

6. Stanković, LJ. Time-frequency signal analysis with applications [Text] / LJ. Stanković, M. Daković, T. Thayaparan. – Arthec House, 2014. – P. 121-130.

7. Marchand, S. The Simplest Analysis Method for Non-Stationary Sinusoidal Modeling [Text] / S. Marchand // In Proceedings of the Digital Audio Effects (DAFx'12). Conference, September 2012. – P. 23-26,

8. Time-frequency reassignment and synchrosqueezing: An overview [Text] / F. Auger, P. Flandrin, Y-T. Lin, S. McLaughlin, S. Meignen, T. Oberlin, H-T. Wu // IEEE Signal Processing Magazine. –2013. – Vol. 30, No. 6. – P. 32-41, 2013.

9. Oberlin, T. A novel Time-Frequency technique for multicomponent signal denoising [Text] / T. Oberlin, S. Meignen, S. McLaughlin // European Signal Processing Conference (EUSIPCO), Marrakech, Morocco, Sept. 9-13, 2013. – P. 650-655.

10. Image denoising by sparse 3D transform-domain collaborative filtering [Text] / K. Dabov, A. Foi, V. Katkovnik, K. Egiazarian // IEEE Transactions on Image Processing. – Aug. 2007. – Vol. 16, No. 8. – P. 2080-2095.

11. A method for predicting denoising efficiency for color images [Text] / O. S. Rubel, R. O. Kozhemiakin, S. S. Krivenko, V. V. Lukin // Proc. of IEEE 35th International Conference on Electronics and Nanotechnology (ELNANO), 2015. – P. 304-309.

12. Time–frequency formulation, design, and implementation of time-varying optimal filters for signal estimation [Text] / F. Hlawatsch, G. Matz, H. Kirchauer, W. Kozek // IEEE Transactions on Signal Processing. – May 2000. – Vol. 48, No. 5. – P. 1417-1432.

13. Jovanovski, S. Signal adaptive pipelined hardware design of time-varying optimal filter for highly nonstationary FM signal estimation [Text] / S. Jovanovski, V. N. Ivanović // Journal of Signal Processing Systems. – 2011. – Vol. 62, No. 3. – P. 287–300.

14. Stanković, LJ. On the time-frequency analysis based filtering [Text] / LJ. Stanković // Annales des Telecommunications. – May 2000. – Vol. 55, No. 5-6. –P. 216-225.

15. Stanković, LJ. Unified approach to the noise analysis in the spectrogram and Wigner distribution [Text] / LJ. Stanković, V. N. Ivanović, Z. Petrović // Annales des Telecommunications. – 1996. – Vol. 51, Nov./Dec., No. 11/12. – P. 585-594.

16. Stanković, LJ. Wigner distribution of noisy signals [Text] / LJ. Stanković, S. Stanković // IEEE

Transactions on Signal Processing. – Feb. 1993. – Vol. 41, No. 2. – P. 956-960.

17. Stanković, LJ. Performance of spectrogram as IF estimator [Text] / LJ. Stanković, M. Daković, V. N. Ivanović // Electronics Letters. – June 2001. – Vol. 37, No. 12. – P. 797-799.

18. Prediction of filtering efficiency for DCT-based image denoising [Text] / S. Abramov, S. Krivenko, A. Roenko, V. Lukin, I. Djurovic, M. Chobanu // In Proc. of MECO, 2013. – P. 97-100.

19. Buades, A. A non-local algorithm for image denoising [Text] / A. Buades, B. Coll, J.-M. Morel // IEEE Computer Society Conference Computer Vision and Pattern Recognition. – June 2005. – Vol. 2. – P. 60-65.

20. Lebrun, M. An analysis and implementation of the BM3D image denoising method [Electronic resource] / M. Lebrun // Image Processing online. – 2012. – Vol. 2. – P. 175-213. – Available at: http://dx.doi.org/10.5201/ipol.2012.l-bm3d. (accessed 22.09.2016).

21. Stockwell, R. G. Localization of the complex spectrum: the S transform [Text] / R. G. Stockwell, L. Mansinha, R. P Lowe // IEEE Transactions on Signal Processing. – Apr. 1996. – Vol. 44, No. 4. – P. 998-1001.

22. Boashash, B. Note on the Use of the Wigner Distribution for Time Frequency Signal Analysis [Text] / B. Boashash // IEEE Transactions on ASSP. – Sept. 1988. – Vol. 36, No. 9. – P. 1518–1521.

23. Parameter Estimation of Signals in Random Noise: An Approach Using Psedo-Wigner Distribution [Text] / H. Ijima, A. Ohsumi, I. Djurović, H. Sato, H. Okura // Trans. IEICE (The Institute of Electronics, Information and Communication Engineers). – 2003. – Vol. J86-A, No. 11. – P.1158-1169.

24. Ohsumi, A. High resolution detector for signals in random noise using wavelet-based Wigner distribution [Text] / A. Ohsumi, H. Ijima, T. Sodeoka // In Proc. of ICASSP 2000. – P. 596-599.

25. Ivanović, V. N. Performance of Quadratic Time-Frequency Distributions as Instantaneous Frequency Estimators [Text] / V. N. Ivanović, M. Daković, and LJ. Stanković // IEEE Transactions on Signal Processing. – Jan. 2003. – Vol. 51, No. 1. – P. 77-89.

26. Stanković, LJ. A method for time-frequency signal analysis [Text] / LJ. Stanković IEEE Transactions on Signal Processing. – Jan. 1994. – Vol. 42, No. 1. – P. 225-229.

27. Elad, M. Sparse and Redundant Representations. From Theory to Applications in Signal and Image [Text] / M. Elad // Processing. Springer Science+Business Media, LLC. – 2010. – P. 212-230.

28. Arce, G. R. Nonlinear Signal Processing: A Statistical Approach [Text] / G. R. Arce. – Wiley-Interscience, 2005. – P. 157-160.

29. Estimation of parameters for generalized Gaussian distribution [Text] / A. A. Roenko, V. V. Lukin, I. Djurović, M. Simeunović // Proceedings of 2014 International Symposium on Communications, Control, and Signal Processing: Special Session on Information Theoretic Methods in Signal Processing, May 21-23, Athens, Greece, 2014. – P. 376-379.

30. New Estimators for Tail Heaviness Parameter of Generalized Gaussian Distribution [Text] / A. Roenko, D. Kurkin, V. Lukin, I. Djurovic // Proceedings of MECO, Bar, Montenegro, June 19-21, 2012. – P. 588-591.

31. Adaptive DCT-based filtering of images corrupted by spatially correlated noise [Text] / V. Lukin, N. Ponomarenko, K. Egiazarian, J. Astola // Proc. SPIE Conference Image Processing: Algorithms and Systems VI. – 2008. – Vol. 6812. – P. 918-924.

32. Lee, J. S. Digital Image Smoothing and the Sigma Filter [Text] / J. S. Lee // Computer Vision, Graphics, and Image Processing. – 1983. – P. 255–269.

33. Sendur, L. Bivariate shrinkage with local variance estimation [Text] / L. Sendur, I. W. Selesnick // IEEE Signal Processing Letters. – 2002. – Vol. 9, No. 12. – P. 438-441.

34. Automatic estimation and removal of noise from a single image [Text] / C. Liu, R. Szeliski, S. B. Kang, C. L. Zitnick, W. T. Freeman // IEEE Transactions on Pattern Analysis and Machine Intelligence. – 2008. – Vol. 30, No 2. –P. 299-314.

35. Solbo, S. Homomorphic Wavelet-based Statistical Despeckling of SAR Images [Text] / S. Solbo, T. Eltoft // IEEE Trans. on Geosc. and Remote Sensing. – 2004. – Vol. GRS-42, No. 4. – P. 711-721.

36. Secrets of Image Denoising Cuisine [Text] / M. Lebrun, M. Colom, A. Buades, J. M. Morel // In Acta Numerica. – 2012. – No. 21. – P. 475-576.

37. Locally Adaptive DCT Filtering for Signal-Dependent Noise Removal [Text] / R. Oktem, K. Egiazarian, V. Lukin, N. Ponomarenko, O. Tsymbal // EURASIP Journal on Advances in Signal Processing. – 2007. – P. 478-490.

38. A non-Parametric Approach for the Estimation of Intensity-Frequency Dependent Noise [Text] / M. Colom, M. Lebrun, A. Buades, J. M. Morel // In IEEE International Conference on Image Processing (ICIP). – 2014. – P. 345-360.
Doi: 10.1109/ICIP.2014.7025865,

39. Astola, J. Fundamentals of nonlinear digital filtering [Text] / J. Astola, P. Kuosmanen. – Boca Raton (USA) : CRC Press LLC, 1997. – P. 176-185.

40. Digital adaptive robust algorithms for radar image filtering [Text] / V. V. Lukin, V. P. Melnik, A. B. Pogrebniak, A. A. Zelensky, K. P. Saarinen, J. T. Astola, Journal of Electronic Imaging. – 1996. – Vol. 5, No. 3. – P. 410-421.

41. Local Activity Indicators: Analysis and Application to Hard-Switching Adaptive Filtering of Images [Text] / V. P. Melnik, V. V. Lukin, A. A. Zelensky, J. T. Astola, P. Kuosmanen // Optical Engineering Journal. – August 2001. – Vol. 40, No. 8. – P. 1441-1455.

42. Baraniuk, R. Wavelet Soft-thresholding of Time-Frequency Representations [Text] / R. Baraniuk // Proceedings of ICIP. – 1994. – Vol. 1. – P. 71-74.

43. Mallawaarachchi, A. Spectrogram denoising and automated extraction of the fundamental frequency

variation of dolphin whistles [Text] / A. Mallawaarachchi, S. Ong // Journal of Acoustic Society of America. – 2008. – Vol. 24, No. 2. – P. 1159-1170.

44. Discrete cosine transform-based local adaptive filtering of images corrupted by nonstationary noise [Text] / V. Lukin, D. Fevralev, N. Ponomarenko, S. Abramov, O. Pogrebnyak, K. Egiazarian, J. Astola // Electronic Imaging Journal. – April-June 2010. – Vol. 19, No. 2, 1. – P. 443-450.

45. Efficiency analysis of DCT-based filters for color image database [Text] / D. Fevralev, V. Lukin, N. Ponomarenko, S. Abramov, K. Egiazarian, J. Astola // Proceedings of SPIE Conference Image Processing: Algorithms and Systems VII, San Francisco, USA. – 2011. – Vol. 7870. – P. 953-964.

46. Suoranta, R. Amplitude domain approach to digital filtering. Theory and applications [Text] : Thesis for the degree of Doctor of Technology / R. Suoranta. – Tampere (Finland, Tampere University of Technology), 1995. – P. 55-67.

47. Sarjanoja, S. BM3D image denoising using heterogeneous computing platforms [Text] : M.Sc. / S. Sarjanoja // Thesis, University of Oulu, March 2015. – P. 34-40.

48. Image and video denoising by sparse 3D transform-domain collaborative filtering [Electronic resource]. – Available at: http://www.cs.tut.fi/~foi/GCF-BM3D/. (accessed 22.09.2016).

References (BSI)

1. Gröchenig, K. *Foundations of Time-Frequency Analysis*. Boston, Birkhäuser Publ., 2001, pp. 30-40.

2. Sejdić, E., Djurović, I., Jiang, J. Time-frequency feature representation using energy concentration: An overview of recent advances. *Digital Signal Processing*, vol. 19, no. 1, Jan. 2009, pp. 153-183.

3. Papandreou-Suppappola, A. *Applications in Time-Frequency Signal Processing*, CRC Press Publ., 2002. 432 p.

4. Jones, D. L., Parks, T. W. A high resolution data-adaptive time-frequency representation. *IEEE Trans. on ASSP*, vol. 38, no. 12, Dec. 1990, pp. 2127-2135.

5. Amin, M. G. Minimum-variance time-frequency distribution kernels for signals in additive noise. *IEEE Trans. Signal Processing*, vol. 44, no. 9, Sept. 1996, pp. 2352-2356.

6. Stanković, L. J., Daković, M., Thayaparan, T. *Time-frequency signal analysis with applications*, Arthec House Publ., 2014, pp. 121-130.

7. Marchand, S. The Simplest Analysis Method for Non-Stationary Sinusoidal Modeling. *In Proceedings of the Digital Audio Effects (DAFx'12) Conference*, September 2012, pp. 23-26.

8. Auger, F., Flandrin, P., Lin, Y-T., McLaughlin, S., Meignen, S., Oberlin, T., Wu, H-T. Time-frequency reassignment and synchrosqueezing: An overview, *IEEE Signal Processing Magazine*, vol. 30, no. 6, 2013, pp. 32-41.

9. Oberlin, T., Meignen, S., McLaughlin, S. A novel Time-Frequency technique for multicomponent signal denoising. *European Signal Processing Conference (EUSIPCO)*, Marrakech, Morocco, Sept. 9-13, 2013, pp. 650-655.

10. Dabov, K., Foi, A., Katkovnik, V., Egiazarian, K. Image denoising by sparse 3D transform-domain collaborative filtering. *IEEE Transactions on Image Processing*, vol. 16, no. 8, Aug. 2007, pp. 2080-2095.

11. Rubel, O. S., Kozhemiakin, R. O., Krivenko, S. S., Lukin, V. V. A method for predicting denoising efficiency for color images. *Proc. of IEEE 35th International Conference on Electronics and Nanotechnology (ELNANO)*, 2015, pp. 304-309.

12. Hlawatsch, F., Matz, G., Kirchauer, H., Kozek, W. Time–frequency formulation, design, and implementation of time-varying optimal filters for signal estimation. *IEEE Transactions on Signal Processing,* vol. 48, no. 5, May 2000, pp. 1417-1432.

13. Jovanovski, S., Ivanović, V. N. Signal adaptive pipelined hardware design of time-varying optimal filter for highly nonstationary FM signal estimation. *Journal of Signal Processing Systems*, vol. 62, no. 3, 2011, pp. 287–300.

14. Stanković, LJ. On the time-frequency analysis based filtering. *Annales des Telecommunications*, vol. 55, no. 5-6, May 2000, pp. 216-225.

15. Stanković, LJ., Ivanović, V. N., Petrović Z. Unified approach to the noise analysis in the spectrogram and Wigner distribution. *Annales des Telecommunications*, vol. 51, Nov./Dec., no. 11/12, 1996, pp. 585-594.

16. Stanković, LJ., Stanković, S. Wigner distribution of noisy signals. *IEEE Transactions on Signal Processing,* vol. 41, no. 2, Feb. 1993, pp. 956-960.

17. Stanković, LJ., Daković, M., Ivanović, V. N. Performance of spectrogram as IF estimator. *Electronics Letters*, vol. 37, no. 12, June 2001, pp. 797-799.

18. Abramov, S., Krivenko, S., Roenko, A., Lukin, V., Djurovic, I., Chobanu, M. Prediction of filtering efficiency for DCT-based image denoising. *In Proc. of MECO*, 2013, pp. 97-100.

19. Buades, A., Coll, B., Morel, J.-M. A non-local algorithm for image denoising. *IEEE Computer Society Conference Computer Vision and Pattern Recognition*, vol. 2, June 2005, pp. 60-65.

20. Lebrun, M. An analysis and implementation of the BM3D image denoising method. *Image Processing online*, vol. 2, 2012, pp. 175-213. Available at: http://dx.doi.org/10.5201/ipol.2012.l-bm3d. (accessed 22.09.2016)

21. Stockwell, R. G., Mansinha, L., Lowe, R. P. Localization of the complex spectrum: the S transform. *IEEE Transactions on Signal Processing*, vol. 44, no. 4, Apr. 1996, pp. 998-1001.

22. Boashash, B. Note on the Use of the Wigner Distribution for Time Frequency Signal Analysis. *IEEE Transactions on ASSP*, vol. 36, no. 9, Sept. 1988, pp. 1518–1521.

23. Ijima, H., Ohsumi, A., Djurović, I., Sato, H., Okura, H. Parameter Estimation of Signals in Random Noise: An Approach Using Psedo-Wigner Distribution. *Trans. IEICE (The Institute of Electronics, Information and Communication Engineers)*, vol. J86-A, no. 11, 2003, pp. 1158-1169.

24. Ohsumi, A., Ijima, H., Sodeoka, T. High resolution detector for signals in random noise using wavelet-based Wigner distribution. *In Proc. of ICASSP 2000*, pp. 596-599.

25. Ivanović, V. N., Daković, M., Stanković, LJ. Performance of Quadratic Time-Frequency Distributions as Instantaneous Frequency Estimators. *IEEE Transactions on Signal Processing*, vol. 51, no. 1, Jan. 2003, pp. 77-89.

26. Stanković, LJ. A method for time-frequency signal analysis. *IEEE Transactions on Signal Processing*, vol. 42, no. 1, Jan. 1994, pp. 225-229.

27. Elad, M. Sparse and Redundant Representations. From Theory to Applications in Signal and Image Processing. *Springer Science+Business Media, LLC,* 2010, pp. 212-230.

28. Arce, G. R. *Nonlinear Signal Processing: A Statistical Approach*. Wiley-Interscience Publ., 2005, pp. 157-160.

29. Roenko, A. A., Lukin, V. V., Djurović, I., Simeunović, M. Estimation of parameters for generalized Gaussian distribution. *Proceedings of 2014 International Symposium on Communications, Control, and Signal Processing: Special Session on Information Theoretic Methods in Signal Processing*, May 21-23, Athens, Greece, 2014, pp. 376-379.

30. Roenko, A., Kurkin, D., Lukin, V., Djurovic, I. New Estimators for Tail Heaviness Parameter of Generalized Gaussian Distribution. *Proceedings of MECO*, Bar, Montenegro, June 19-21, 2012, pp. 588-591.

31. Lukin, V., Ponomarenko, N., Egiazarian, K., Astola, J. Adaptive DCT-based filtering of images corrupted by spatially correlated noise. *Proc. SPIE Conference Image Processing: Algorithms and Systems VI*, vol. 6812, 2008, pp. 918-924.

32. Lee, J. S. Digital Image Smoothing and the Sigma Filter. *Computer Vision, Graphics, and Image Processing*, 1983, pp. 255–269.

33. Sendur, L., Selesnick, I. W. Bivariate shrinkage with local variance estimation. *IEEE Signal Processing Letters*, vol. 9, no. 12, 2002, pp. 438-441.

34. Liu, C., Szeliski, R., Kang, S. B., Zitnick, C. L., Freeman, W. T. Automatic estimation and removal of noise from a single image. *IEEE Transactions on Pattern Analysis and Machine Intelligence*, vol. 30, no. 2, 2008, pp. 299-314.

35. Solbo, S., Eltoft, T. Homomorphic Wavelet-based Statistical Despeckling of SAR Images. *IEEE Trans. on Geosc. and Remote Sensing*, vol. GRS-42, no. 4, 2004, pp. 711-721.

36. Lebrun, M., Colom, M., Buades, A., Morel, J. M. Secrets of Image Denoising Cuisine. *In Acta Numerica*, no. 21, 2012, pp. 475-576.

37. Oktem, R., Egiazarian, K., Lukin, V., Ponomarenko, N., Tsymbal, O. Locally Adaptive DCT Filtering for Signal-Dependent Noise Removal. *EURASIP Journal on Advances in Signal Processing*, 2007, pp. 478-490.

38. Colom, M., Lebrun, M., Buades, A., Morel, J. M. A non-Parametric Approach for the Estimation of Intensity-Frequency Dependent Noise. *In IEEE International Conference on Image Processing (ICIP)*, 2014, pp. 345-360. Doi: 10.1109/ICIP.2014.7025865.

39. Astola, J., Kuosmanen, P. *Fundamentals of nonlinear digital filtering*. Boca Raton (USA), CRC Press LLC, 1997, pp. 176-185.

40. Lukin, V. V., Melnik, V. P., Pogrebniak, A. B., Zelensky, A. A., Saarinen, K. P., Astola, J. T. Digital adaptive robust algorithms for radar image filtering. *Journal of Electronic Imaging*, vol. 5, no. 3, 1996, pp. 410-421.

41. Melnik, V. P., Lukin, V. V., Zelensky, A. A., Astola, J. T., Kuosmanen, P. Local Activity Indicators: Analysis and Application to Hard-Switching Adaptive Filtering of Images. *Optical Engineering Journal*, August 2001, vol. 40, no. 8, pp. 1441-1455.

42. Baraniuk, R. Wavelet Soft-thresholding of Time-Frequency Representations. *Proceedings of ICIP*, 1994, vol. 1, pp. 71-74.

43. Mallawaarachchi, A., Ong, S. Spectrogram denoising and automated extraction of the fundamental frequency variation of dolphin whistles. *Journal of Acoustic Society of America*, vol. 24, no. 2, 2008, pp. 1159-1170.

44. Lukin, V., Fevralev, D., Ponomarenko, N., Abramov, S., Pogrebnyak, O., Egiazarian, K., Astola, J. Discrete cosine transform-based local adaptive filtering of images corrupted by nonstationary noise. *Electronic Imaging Journal*, vol. 19, no. 2, 1, April-June 2010, pp. 443-450.

45. Fevralev, D., Lukin, V., Ponomarenko, N., Abramov, S., Egiazarian, K., Astola, J. Efficiency analysis of DCT-based filters for color image database. *Proceedings of SPIE Conference Image Processing: Algorithms and Systems VII*, San Francisco, USA, vol. 7870, 2011, pp. 953-964.

46. Suoranta, R. Amplitude domain approach to digital filtering. Theory and applications. *Thesis for the degree of Doctor of Technology*, Tampere (Finland, Tampere University of Technology), 1995, pp. 55-67.

47. Sarjanoja, S. *BM3D image denoising using heterogeneous computing platforms*. M.Sc. Thesis, University of Oulu, March 2015, pp. 34-40.

48. Image and video denoising by sparse 3D transform-domain collaborative filtering. Available at: http://www.cs.tut.fi/~foi/GCF-BM3D/ (accessed 22.09.2016).

Поступила в редакцию 17.11.2016, рассмотрена на редколлегии 09.12.2016

ВОССТАНОВЛЕНИЕ ЧАСТОТНО-ВРЕМЕННЫХ ПРЕДСТАВЛЕНИЙ: ПОДХОД С ИСПОЛЬЗОВАНИЕМ МЕТОДОВ ФИЛЬТРАЦИИ ИЗОБРАЖЕНИЙ

И. Джурович, В. Лукин, А. Роенко

Рассмотрена задача повышения качества частотно-временных представлений, полученных S-методом, при помощи современных локальных и нелокальных цифровых фильтров, которые разработаны и применяются в области обработки изображений. Актуальность задачи связана с необходимостью наличия частотно-временных фильтров для обработки нестационарных частотно-модулированных сигналов. В работе рассмотрено применение медианного фильтра как представителя класса локальных пространственных фильтров, фильтрации на основе ДКП в качестве представителя методов фильтрации на основе ортогональных преобразований, а также BM3D-фильтра как одного из лучших на данный момент среди нелокальных методов. Показано, что шум в частотно-временных распределениях, полученных с помощью S-метода, имеет сложную структуру, а именно, может в ряде ситуаций иметь негауссово распределение значений, а также обладать пространственной корреляцией. Показано, что применение описанных выше фильтров в данных помеховых условиях приводит к неудовлетворительным результатам. Предложено несколько модификаций рассматриваемых методов, эффективность работы которых проанализирована с точки зрения интегральных и локальных параметров. Показано, что наилучших результатов в шумоподавлении позволяет достичь модификация BM3D-фильтра. Однако платой за улучшения является потеря точности в представлении слабых компонент полезного сигнала.

Ключевые слова: частотно-временное распределение; S-метод; цифровая обработка изображений; ДКП-фильтр; BM3D-фильтр.

ВІДНОВЛЕННЯ ЧАСТОТНО-ЧАСОВИХ ПРЕДСТАВЛЕНЬ: ПІДХІД З ЗАСТОСУВАННЯМ МЕТОДІВ ФІЛЬТРАЦІЇ ЗОБРАЖЕНЬ

І. Джуровіч, В. Лукін, О. Роєнко

Розглянуто задачу підвищення якості частотно-часових представлень, що отримано S-методом, за допомогою сучасних локальних та нелокальних цифрових фільтрів, які розроблено та застосовано у галузі обробки зображень. Актуальність задачі пов'язана з необхідністю наявності частотно-часових фільтрів для обробки нестаціонарних частотно-модульованих сигналів. У роботі розглянуто застосування медіанного фільтру як представника класу локальних просторових фільтрів, фільтрації на базі ДКП у якості представника методів фільтрації на базі ортогональних перетворень, а також BM3D-фільтра як одного з найкращих на даний час серед нелокальних методів. Показано, що шум у частотно-часових розподілах, що отримано за допомогою S-методу, має складну структуру, а саме, може у ряді випадків мати негаусів розподіл значень, а також мати просторову кореляцію. Наведено, що застосування описаних вище фільтрів у даних завадових умовах приводить до незадовільних результатів. Запропоновано декілька модифікацій методів, що розглянуто, ефективність роботи яких проаналізовано з точки зору інтегральних та локальних параметрів. Показано, що найкращі результати у шумопридушенні дозволяє досягти модифікація BM3D-фільтру. Проте платою за покращення є втрата точності у представленні слабких компонент корисного сигналу.

Ключові слова: Частотно-часовий розподіл; S-метод; цифрова обробка зображень; ДКП-фільтр; BM3D-фільтр.

Джурович Игорь – профессор Электротехнического факультета, университет Черногории, Подгорица, Черногория, и Института передовых информационных и связных технологий, Подгорица, Черногория, e-mail: igordj@ac.me.

Лукин Владимир – профессор, заведующий каф. приема, передачи и обработки сигналов, Национальный аэрокосмический университет им. Н. Е. Жуковского «Харьковский авиационный институт», Харьков, Украина, e-mail: lukin@ai.kharkov.com.

Роенко Алексей – доцент каф. приема, передачи и обработки сигналов, Национальный аэрокосмический университет им. Н. Е. Жуковского «Харьковский авиационный институт», Харьков, Украина, e-mail: roenkomail@mail.ru.

Djurović Igor – Professor of the Electrical Engineering Department, University of Montenegro, Podgorica, Montenegro, and of the Institute for Cutting Edge Information and Communication Technologies, Podgorica, Montenegro, e-mail: igordj@ac.me.

Lukin Vladimir – Professor, Head of the Dept. of Signal Reception, Transmission and Processing, National Aerospace University named after N. Ye. Zhukovsky «Kharkov Aviation Institute», Kharkov, Ukraine, e-mail: lukin@ai.kharkov.com.

Roenko Alexey – Associate professor of the Dept. of Signal Reception, Transmission and Processing, National Aerospace University named after N. Ye. Zhukovsky «Kharkov Aviation Institute», Kharkov, Ukraine, e-mail: roenkomail@mail.ru.